Nanochem Res 8(2): 106-116 Spring 2023

RESEARCH PAPER

Theoretical Investigation of Amantadine Adsorption on Sc-, Ti-, and Zn-Boron Nitride Nanosheets: DFT, NBO, and QTAIM

Ebrahim Saedi Khosroshahi[1], Ladan Edjlali[1], Farnaz Behmagham[2,*], Mirzaagha Babazadeh[1], Elnaz Ghasemi[1]

[1] Department of Chemistry, Tabriz Branch, Islamic Azad University, Tabriz, Iran

[2] Department of Chemistry, Miandoab Branch, Islamic Azad University, Miandoab, Iran

ARTICLE INFO

Article History:
Received 18 Nov 2022
Accepted 18 Feb 2023
Published 06 Mar 2023

Keywords:
Amantadine
Adsorption
Detection
Transition metal doped BN nanosheet
DFT

ABSTRACT

In this work, the potentials of Sc-, Ti-, and Zn-doped BN nanosheets for adsorbing and detecting the amantadine drug were studied by using density functional theory (DFT), natural bond orbital (NBO), and quantum theory of atoms in molecules (QTAIM). The amantadine adsorption on the considered doped BNNSs was chemisorption. The strongest adsorption was related to the amantadine adsorption on Sc-doped BNNS. Among the considered doped BNNSs, only Sc-doped BNNS can be employed as a suitable electronic conductivity detector for amantadine in the environment. In addition, all the considered doped BNNSs, may be proper for work function type in detecting the drug.

How to cite this article
Saedi Khosroshahi E., Edjlali L., Behmagham F., Babazadeh M., Ghasemi E., Theoretical Investigation of Amantadine Adsorption on Sc-, Ti-, and Zn-Boron Nitride Nanosheets: DFT, NBO, and QTAIM. Nanochem Res, 2023; 8(2): 106-116
DOI: 10.22036/ncr.2023.02.003

INTRODUCTION

Pharmaceuticals play a significant role in improving human health and the quality of life, yet the release of unused pharmaceuticals in the environment can have devastating impacts on ecosystems. The most important sources of spreading pharmaceuticals in the environment include excreting active ingredients of pharmaceuticals from the bodies of humans or animals, improperly getting rid of unused or expired medicines, and releasing active ingredients in nearby waterways [1-3]. Due to their potentially devastating impacts, sensing and removing pharmaceuticals and their active ingredients accumulated in soil, river, and lake water is essential. Amantadine is a tricyclic amine employed for treating dyskinesia associated with parkinsonism and influenza type A [4]. Further, this drug is used for treating pain in dogs and cats [5, 6]. A small amount of amantadine is metabolized in the body and the rest (about 90%) is excreted unchanged by kidneys in urine [7].

Nanostructures have attracted great attention to be employed as adsorbents and detectors owing to their highly efficient surface area [8-11]. Parlak and Alver studied the potentials of B, Al, Si, Ga, and Ge-doped C_{60} fullerenes for detecting and adsorbing amantadine [12]. They showed that doped C_{60} fullerenes could be utilized for detecting amantadine. As shown by Noroozi *et. al.*, the adsorption of amantadine on the bowl-like B_{30} nanocluster reduces the E_g of B_{30} by 13.7% which indicates the sensitivity of B_{30} toward amantadine; however, there is a strong attraction between amantadine and B_{30} (-194.2 kj/mol) [13]. The adsorption of amantadine on pristine and Al-doped $B_{12}N_{12}$ and $Zn_{12}O_{12}$ nanocages was investigated by Farmanzadeh and Keyhanian [14]. They demonstrated that amantadine was chemically adsorbed on pristine and doped considered nanocages. Xianghong Sun *et. al.* indicated that $Al_{12}O_{12}$ and $B_{12}N_{12}$ nanocages could be employed

* Corresponding Author Email: *behmagham_farnaz@yahoo.com*

as work function type and conductivity sensors, respectively [15]. Doust Mohammadi and Abdullah investigated amantadine adsorption on pristine, Al-, Ga-, P-, and As-doped boron nitride nanosheets employing several DFT functionals [16]. Based on their calculations, the amantadine adsorption on the pristine nanosheet was a physisorption type, whereas the drug was chemically adsorbed on the doped nanosheets. In another work, they studied the interaction of amantadine with C_{60} and $C_{59}X$ fullerenes (X=Si, Ge, B, Al, Ga, N, P, and As), indicating that $C_{59}X$ fullerenes were more sensitive toward the medication than C_{60} fullerene [17]. The present work aims to study the potentials of Sc-, Ti-, and Zn-doped boron nitride nanosheets for adsorbing and detecting amantadine drug, employing B3LYP and CAM-B3LYP DFT functionals, natural bond orbital (NBO), and quantum theory of atoms in molecules (QTAIM) analyses.

In this study, the used dopant elements have vacant orbitals, thereby they can play Lewis acid role that can interact with elements having the nonbonding pair electrons. Therefore, the novelty of this work was included as follows: (1) choosing the transition metals as the dopant elements which is unprecedented in the literature, (2) discussing two main parameters including E_g and E_{ad} which play the main role in the sensing ability, (3) using the QTAIM method for those system.

COMPUTATIONAL DETAILS

Density functional theory (DFT) through B3LYP hybrid functional [18] accompanied by 6-31G(d) basis set was applied for optimizing the geometries of amantadine, doped boron nitride nanosheets (BNNS), and amantadine-nanosheet complexes. The adsorption energies ($E_{ads}E_{ads}$) between amantadine and doped BNNS were obtained using Eq. (1):

$$E_{ads} = E_{AD-NS} - E_{AD} - E_{NS} + BSSE \quad (1)$$

where $E_{AD-NS}E_{AD-NS}$, $E_{AD}E_{AD}$, and $E_{NS}E_{NS}$ denote the energies of amantadine-nanosheet complexes, amantadine drug, and doped BNNSs, respectively. BSSE stands for the basis set superposition error, calculated by applying Boys-Bernardi method [19]. Furthermore, Eqs. (2) to (5) were used to calculate binding energies, deformation energies of amantadine ($E_{def.AD}$ $E_{def.AD}$) and doped BNNSs ($E_{def.NS}E_{def.NS}$), and total deformation energies of amantadine-nanosheet complexes ($E_{total\ def}E_{total\ def}$), respectively.

$$E_{binding} = E_{AD\ in\ com} + E_{NS\ in\ com} - E_{AD-NS} - BSSE$$

(2)

$$E_{def.AD} = E_{AD\ in\ com} - E_{AD} \quad (3)$$

$$E_{def.NS} = E_{NS\ in\ com} - E_{NS} \quad (4)$$

$$E_{total\ def} = E_{def.AD} + E_{def.NS} \quad (5)$$

where $E_{AD\ in\ com}E_{AD\ in\ com}$ and $E_{NS\ in\ com}$ $E_{NS\ in\ com}$ are the energies of amantadine and doped BNNS in their complex geometries. The adsorption, binding, and deformation energies were calculated using B3LYP and CAM-B3LYP [20] hybrid functionals and 6-31G(d) basis set. All optimization and energy calculations were carried out using Gaussian 09 quantum package [21].

For obtaining the highest occupied molecular orbital (HOMO), the lowest unoccupied molecular orbital (LUMO), and charge transfer, the NBO analysis was performed using NBO3 embedded Gaussian 09 [21]. For characterizing molecular orbitals, the orbital decomposition analysis was carried out using Chemcraft 1.7 [22]. Additionally, GaussSum package was used to draw the density of states (DOS) and partial density of states (PDOS) diagrams [23]. The bandgap energy, fermi level, and work function were calculated by Eqs. (6) to (8):

$$E_g = LUMO - HOMO \quad (6)$$

$$E_f = \frac{1}{2}(LUMO + HOMO) \quad (7)$$

$$\Phi = E_\infty - E_f \xrightarrow{E_\infty \cong 0} - E_f \quad (8)$$

The quantum theory of atoms in molecules (QTAIM) analysis was employed to recognize the nature of the interaction between amantadine and doped BNNSs [24]. QTAIM analysis was conducted by Multiwfn 3.7 [25]. To ensure the global minima for the boron nitride complex rather than a local minimum, the potential energy surface (PES) scans were performed with respect to several dihedral angles (D).

RESULTS AND DISCUSSION

Structure, electrostatic potential, and NBO of amantadine

As shown in Fig. 1, amantadine is an organic compound with a chemical formula C10H17N

Table 1. The formation energy (E_{form}), doping energy (E_{dop}), the HOMO, LUMO, and fermi (E_f) energy levels, Bandgap between HOMO and LUMO (E_g) and work function (Φ) of pristine and Sc-, Ti-, and Zn-doped BNNSs

Nano Sheet	E_{form} (Kcal/mol)	E_{dop} (Kcal/mol)	HOMO (eV)	LUMO (eV)	E_f (eV)	Bandgap (eV)	Φ (eV)
BNNS	-2284.46 (-2104.30)	--	-8.02 (-6.62)	1.39 (0.06)	-3.32 (-3.28)	9.41 (6.68)	3.32 (3.28)
Sc-doped BNNS	-2161.31 (-1987.76)	123.15 (116.54)	-7.72 (-6.24)	-1.11 (-1.97)	-4.42 (-4.11)	6.61 (4.27)	4.42 (4.11)
Ti-doped BNNS	-2160.72 (-1983.12)	123.74 (121.17)	-5.92 (-4.21)	-0.31 (-1.21)	-3.12 (-2.71)	5.61 (3.00)	3.12 (2.71)
Zn-doped BNNS	-2042.48 (-1866.70)	241.98 (237.60)	-7.46 (-6.07)	-3.66 (-4.68)	-5.56 (-5.38)	3.8 (1.39)	5.56 (5.38)

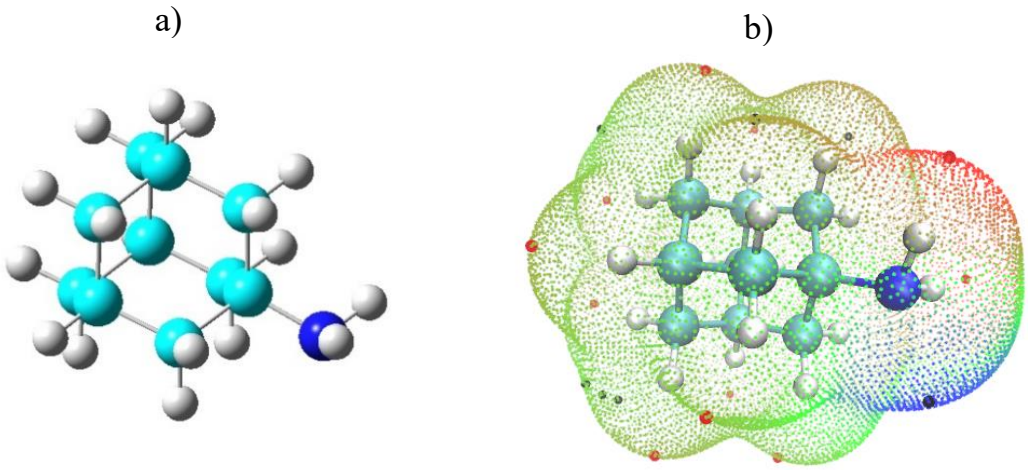

Fig. 1. (a) the structure and (b) the map of electrostatic potential of amantadine

which include three cyclohexane with an amino group substituent. Moreover, Fig. 1 depicts the map of the electrostatic potential (ESP) of amantadine. As shown, the minimum and maximum ESPs are located on nitrogen and hydrogens linked to nitrogen, respectively. The NBO analysis indicated that the minimum and maximum partial charges are related to nitrogen and its linked hydrogens with a partial charge of -0.895 and +0.373 in CAM-B3LYP level (-0.888 and -0.370 in B3LYP level), respectively. The DOS diagram and the shape of HOMO and LUMO obtained in CAM-B3LYP level are shown in Fig. 2. HOMO, LUMO, and bandgap energies of amantadine are -7.82, 3.16, and 10.98 eV, respectively. The orbital decomposition analysis demonstrated that HOMO and LUMO were mainly dominated by occupied p orbitals of N atom and unoccupied s orbitals of N, C, and H atoms, respectively.

Optimized structure and NBO of pristine and SC-, Ti-, and Zn-doped BNNSs

The optimized geometry of the BNNS model consists of 27 pairs of boron and nitrogen atoms organized in 20 hexagonal rings (Fig. 3). Hydrogen atoms were added to 18 edge atoms of the nanosheet, leading to their to saturation. The partial charge of nitrogen and boron atoms (except for edge N and B) are -1.186 to -1.189 and +1.180 to +1.185 in CAM-B3LYP level (-1.171 to -1.174 and +1.166 to +1.170 in B3LYP level), respectively, indicating the ionic nature of B-N bonds. The DOS diagram and the shape of HOMO and LUMO of BNNS at CAM-B3LYP level are shown in Fig. 4. Additionally, HOMO, LUMO, bandgap, fermi level, and work function of BNNS are listed in Table 1. Based on orbital decomposition analysis, the occupied p orbitals of N atoms and unoccupied p orbitals of edge B atoms mainly form HOMO and LUMO of BNNS, respectively.

Sc-, Ti-, and Zn-doped BNNSs were built by replacing one of the B atoms of the central ring with Sc, Ti, and Zn atoms. Fig. 5 shows the geometries of Sc-, Ti-, and Zn-doped BNNSs. As depicted, replacing the boron atom with the dopants deforms the flat structure of the nanosheet. The doping

Table 2. The NBO charge population analysis of pristine and Sc-, Ti-, and Zn-doped BNNSs

Nanosheet	Charges of dopand	Charges of B atoms	Charges of N atoms
BNNS	---	+1.180 to +1.185 (-1.171 to -1.174)	-1.186 to -1.189 (+1.166 to +1.170)
Sc-doped BNNS	+1.730 (+1.669)	+1.143 to 1.187 (+1.132 to +1.161)	-1.191 to -1.249 (-1.175 to -1.221)
Ti-doped BNNS	+1.408 (+1.336)	+1.149 to +1.190 (+1.134 to +1.174)	-1.181 to -1.194 (-1.154 to -1.181)
Zn-doped BNNS	+1.337 (+1.322)	+1.145 to +1.189 (+1.128 to +1.174)	-1.091 to -1.33 (-1.089 to -1.313)

energies (E_{dop}) and formation energies (E_{form}) were obtained by the following formulas:

$$E_{dop} = E_{doped-BNNS} - E_{BNNS} - E_{dopand} + E_B \quad (9)$$

$$E_{form} = E_{doped-BNNS} - 26E_B - E_{dopand} - \frac{27}{2}E_{N2} - \frac{27}{2}E_{H2} \quad (10)$$

where $E_{doped-BNNS}E_{doped-BNNS}$, E_{BNNS} E_{BNNS}, $E_{dopand}E_{dopand}$, E_BE_B, $E_{N2}E_{N2}$, and E_{H2} E_{H2} indicate the energies of doped BNNS, BNNS, isolated dopant atom, isolated B atom, and Nitrogen and Hydrogen molecules. The doping and formation energies are reported in Table 1. As shown, Sc-, Ti-, and Zn-doped BNNSs are highly stable; however, their stability is less than pure BNNS.

Table 2 presents the results of NBO population analysis for pristine and doped BNNSs. As shown in Table 2, replacing a central B atom with transition metal atoms increases charge separation between cations and onions, especially in the vicinity of metal dopant. The PDOS diagrams of Doped BNNSs at CAM-B3LYP level are depicted in Fig. 5. HOMO, LUMO, fermi energy, bandgap, and work function of doped BNNSs are included in Table 1. Based on Table 1 and Fig. 5, the Sc-doping diminished the bandgap energy by decreasing the LUMO level. Based on orbital decomposition analysis, occupied d orbitals of the Sc atom partly contributes to the HOMO level. However, the LUMO mainly is comprised of unoccupied s and p orbitals of the Sc atom. Replacing the B with Ti reduced the bandgap by decreasing the LUMO level and made a new single electron orbital in the vicinity of the fermi level of BNNS. In addition to the unrestricted electron character of Ti-doped BNNSs, there are two kinds of single electron orbitals for electrons with the spin of α and β. HOMO and LUMO are relative to the highest occupied orbital for spin α and the lowest unoccupied orbital for spin β, respectively. The occupied d orbitals of the Ti atom dominate the HOMO level, whereas the LUMO level consists of unoccupied s orbitals associated with unoccupied p and d orbitals of the Ti atom. Similar to Ti-doped BNNS, the molecular orbitals in Zn-doped BNNS are different for electrons with spins of α and β. The HOMO and LUMO of Zn-doped BNNS correspond to the highest occupied and the lowest unoccupied orbitals relative to spin β, respectively. HOMO and LUMO of Zn-doped BNNS are mainly dominated by the occupied and unoccupied p orbitals of N atoms in the vicinity of the Zn atom. The shape of HOMO and LUMO of Sc-, Ti-, and Zn-doped BNNSs are displayed in Fig. 6.

Amantadine adsorption on Sc-, Ti-, and Zn-doped BNNSs

Based on the ESP map of the amantadine drug in Fig. 1, amantadine can be adsorbed on the doped metal of the doped BNNSs from its nitrogen atom. Fig. 7 shows the geometries of amantadine adsorption on the doped BNNSs. In addition, the adsorption and deformation energies are reported in Table 3, indicating that amantadine adsorption on the doped BNNSs has a chemisorption nature [26]. Sc-doped BNNS is the best adsorbent for amantadine among the considered doped BNNSs in this work; this nanosheet experienced the least deformation after adsorbing amantadine. Furthermore, the NBO second-order perturbation theory analysis of Fock matrix and QTAIM analysis were performed to characterize the interaction between amantadine and the doped BNNSs. Table 4 summarizes main electron delocalizations and their 2e-stabilization energies (E(2)) between amantadine and doped BNNSs. As shown, the electron delocalization between the lone pair (LP) of the N atom of amantadine (as donor) and LP* of transition metals is mainly responsible for the

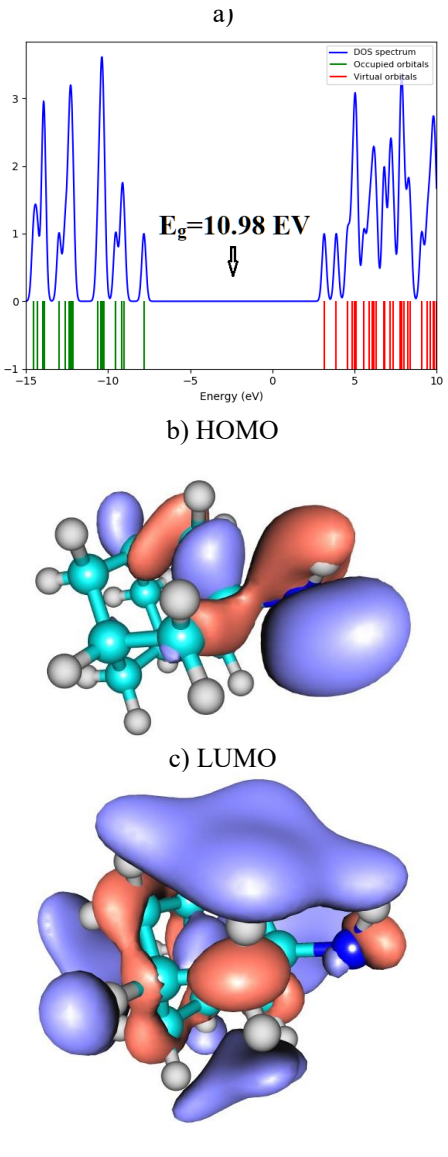

Fig. 2. (a) DOS diagram and (b) the shaape of HOMO and (c) LUMO of Amantadine

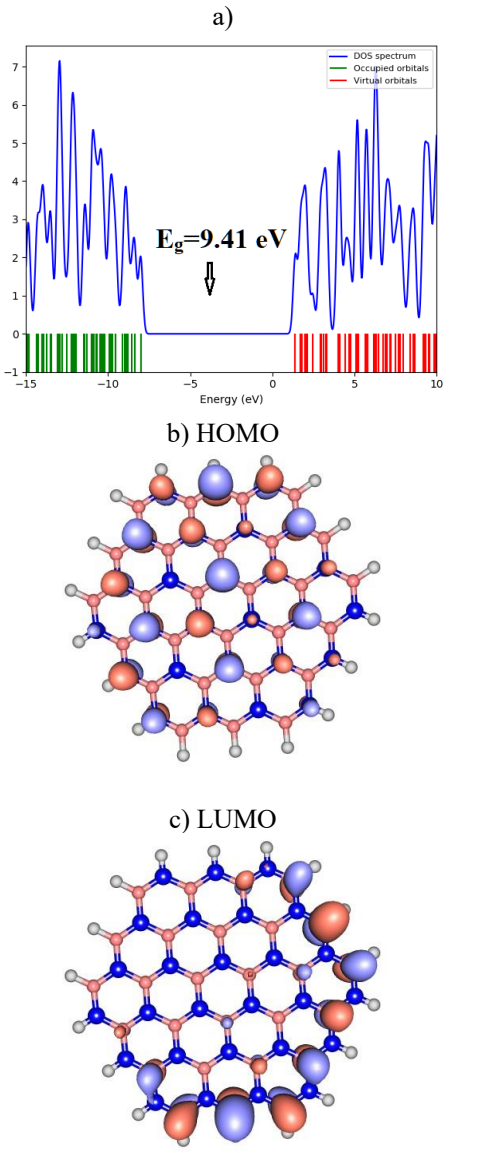

Fig. 4. (a) DOS diagram and the shape of (b) HOMO and (c) LUMO of BN nanosheet

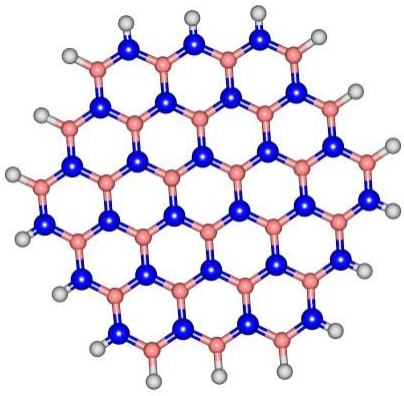

Fig. 3. The structure of BN nanosheet

Table 3. The adsorption, binding, and deformation energies of amantadine on Sc-, Ti-, and Zn-doped BNNSs, and charge transfer from amantadine to the nanosheet

Nanosheet	E_{ads} (Kcal/mol)	E_{bind} (Kcal/mol)	$E_{def,AD}$ (Kcal/mol)	$E_{def,NS}$ (Kcal/mol)	$E_{total\ def}$ (Kcal/mol)	Charge transfer (e)
AD-Sc-doped BNNS	-31.90 (-28.96)	33.70 (30.15)	0.81 (0.65)	0.99 (0.53)	1.80 (1.18)	-0.139 -0.139)
AD-Ti-doped BNNS	-25.82 (-21.89)	32.35 (27.42)	0.93 (0.78)	5.60 (4.75)	6.52 (5.53)	-0.157 (-0.077)
AD-Zn-doped BNNS	-23.63 (-20.10)	30.63 (26.14)	0.70 (0.62)	6.30 (5.41)	7.00 (6.03)	-0.155 (-0.077)

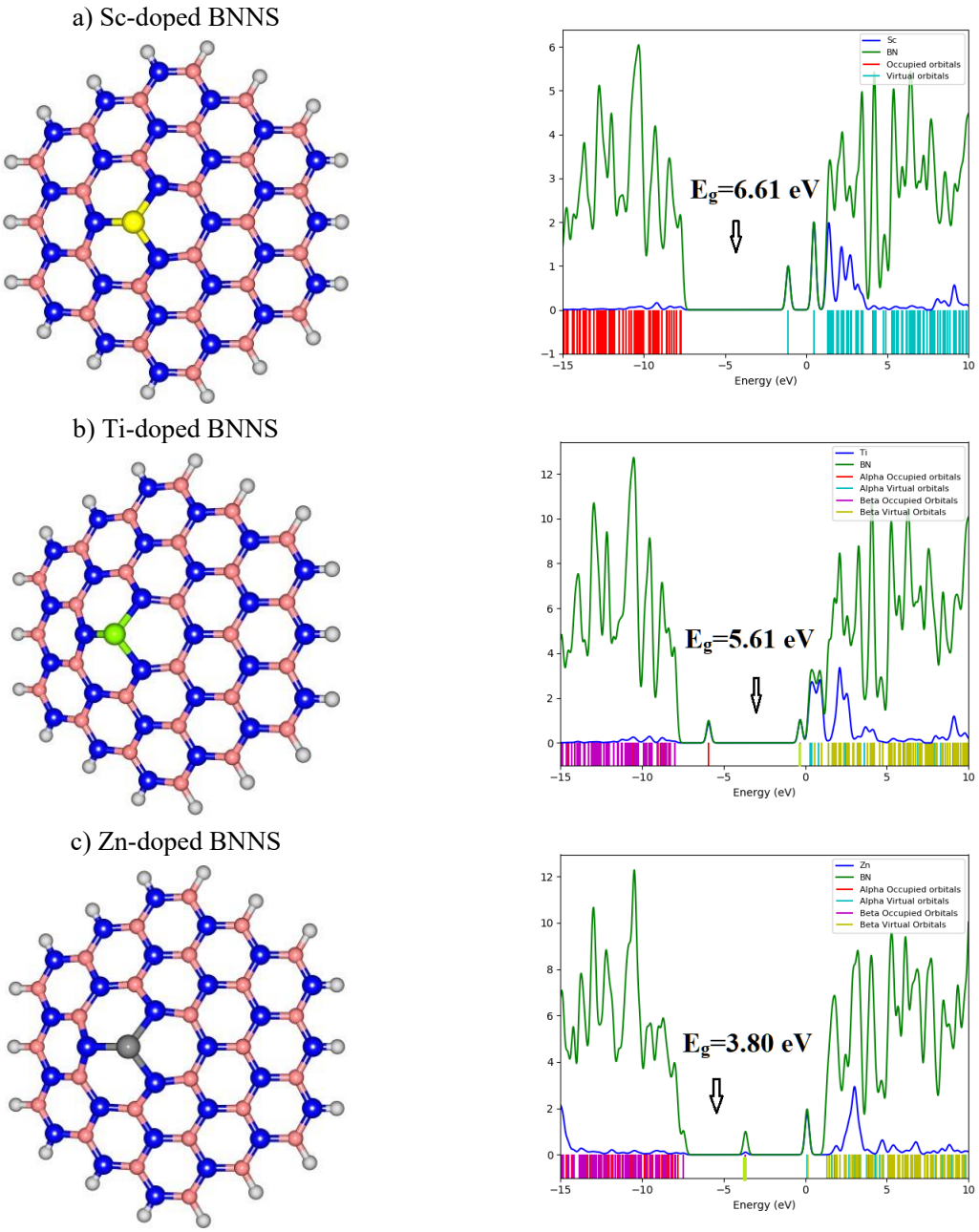

Fig. 5. The structure and PDOS diagrams of (a) Sc-, (b) Ti-, and (c) Zn-doped BNNSs

Table 4. NBO second-order perturbation theory analysis of Fock matrix of amantadine adsorption on Sc-, Ti-, and Zn-doped BNNSs

	donor	acceptor	E(2)/(kcal/mol)
AD-Sc-doped BNNS	LP (N, AD)	LP*(Sc, NS)	56.49
AD-Ti-doped BNNS	LP (N, AD)	LP*(Ti, NS)	33.5
AD-Zn-doped BNNS	LP (N, AD)	LP*(Zn, NS)	29.74
	LP (N, AD)	BD*(N-Zn,NS)	7.09

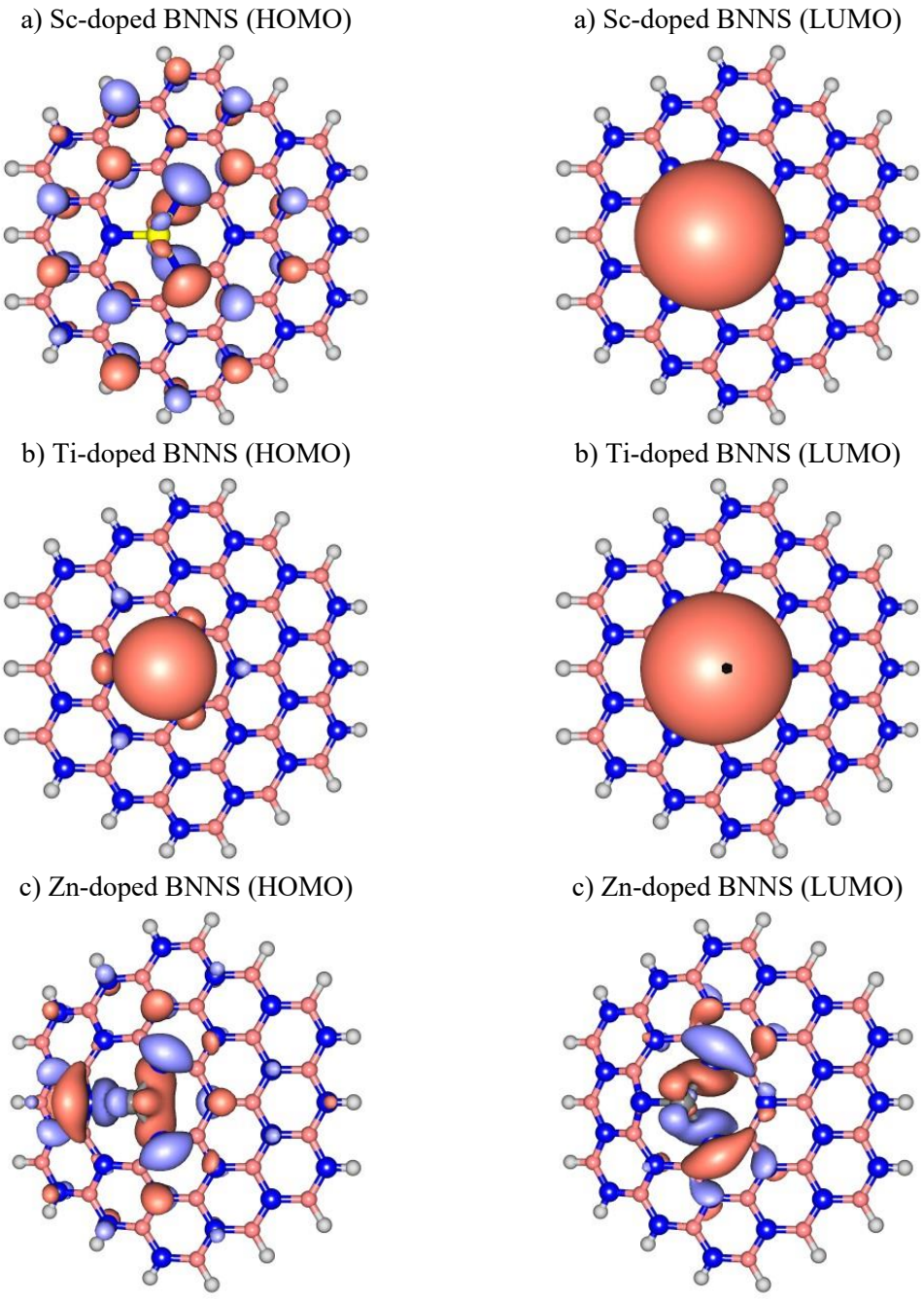

Fig. 6. The shape of HOMO and LUMO of (a) Sc-, (b) Ti-, and (c) Zn-doped BNNSs

Table 5. QTAIM analysis of amantadine adsorption on Sc-, Ti-, and Zn-doped BNNSs

	Critical number	Critical path	ρ	G(r)	V(r)	|V|/G	LOL
AD-Sc-doped BNNS	1	N…Sc	0.0404	0.0393	-0.0362	0.9198	0.2574
	2	C-H...N	0.0068	0.0037	-0.0031	0.8310	0.1583
	3	C-H...N	0.0036	0.0021	-0.0015	0.6990	0.1044
AD-Ti-doped BNNS	1	N…Ti	0.0493	0.0535	-0.0503	0.9410	0.2628
	2	C-H…N	0.0044	0.0026	-0.0019	0.7409	0.1158
AD-Zn-doped BNNS	1	N…Zn	0.0744	0.0884	-0.1159	1.3110	0.2992
	2	C-H...N	0.0070	0.0044	-0.0036	0.8306	0.1451
	3	C-H...N	0.0040	0.0024	-0.0018	0.7189	0.1068

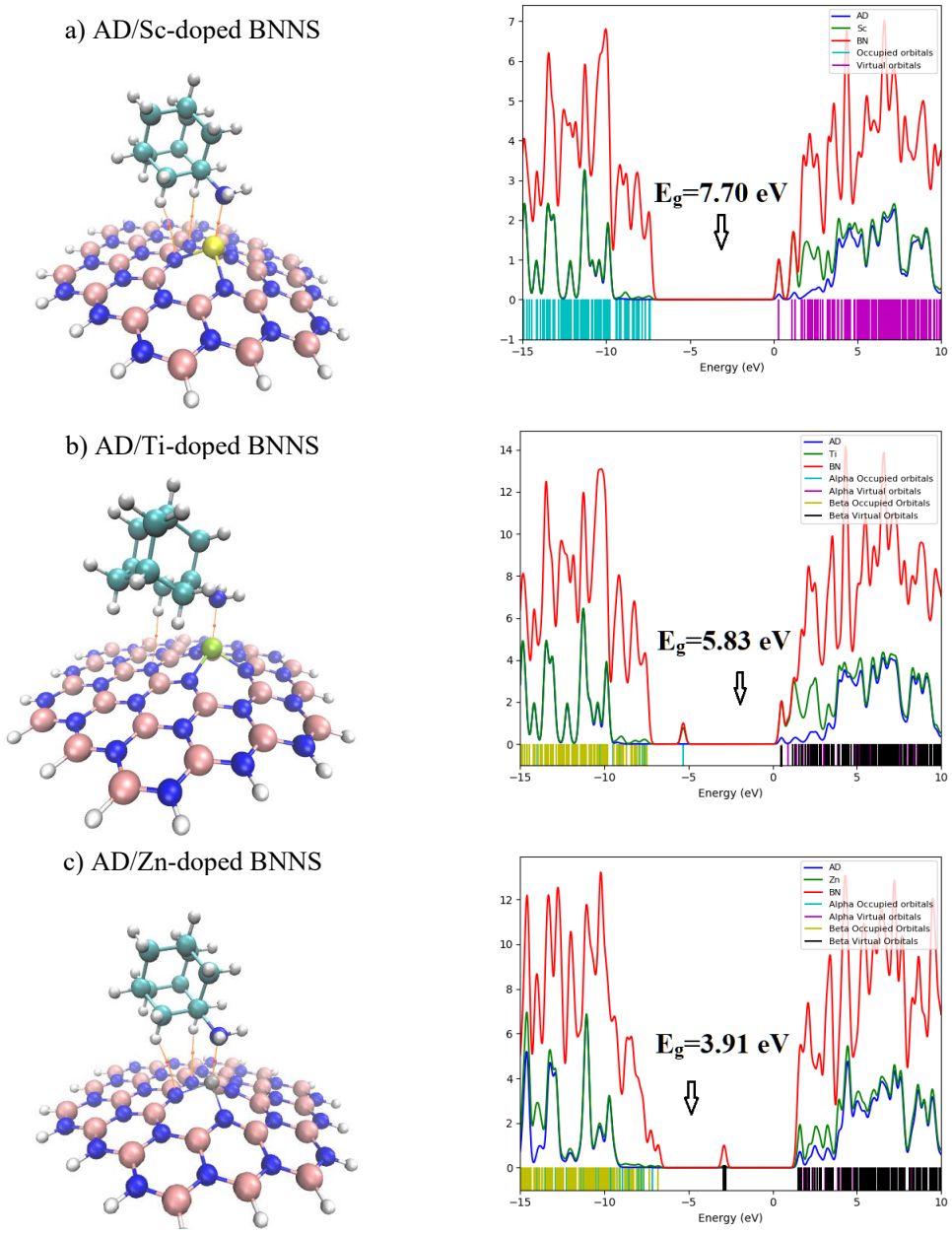

Fig. 7. The structure (containing interaction critical points) and PDOS diagram of the adsorption of amantadine on (a) Sc-, (b) Ti-, and (c) Zn-doped BNNSs

Table 6. the HOMO, LUMO, and fermi (E_f) energy levels, Bandgap between HOMO and LUMO (E_g) and work function (Φ) of Sc-, Ti-, and Zn-doped BNNSs adsorbed amantadine

	HOMO (eV)	LUMO (eV)	E_f (eV)	Bandgap (eV)	Φ (eV)	Bandgap change (%)	Φ change (%)
AD-Sc-doped BNNS	-7.39	0.31	-3.54	7.70	3.54	16.49	-19.82
	(-5.92)	(-0.6)	(-3.26)	(5.32)	(3.26)	(24.59)	(-20.58)
AD-Ti-doped BNNS	-5.32	0.51	-2.41	5.83	2.41	3.92	-22.79
	(-3.45)	(-0.43)	(-1.94)	(3.02)	(1.94)	(0.67)	(-28.41)
AD-Zn-doped BNNS	-6.80	-2.89	-4.85	3.91	4.85	2.89	-12.86
	(-5.42)	(-3.98)	(-4.70)	(1.44)	(4.70)	(3.60)	(-12.56)

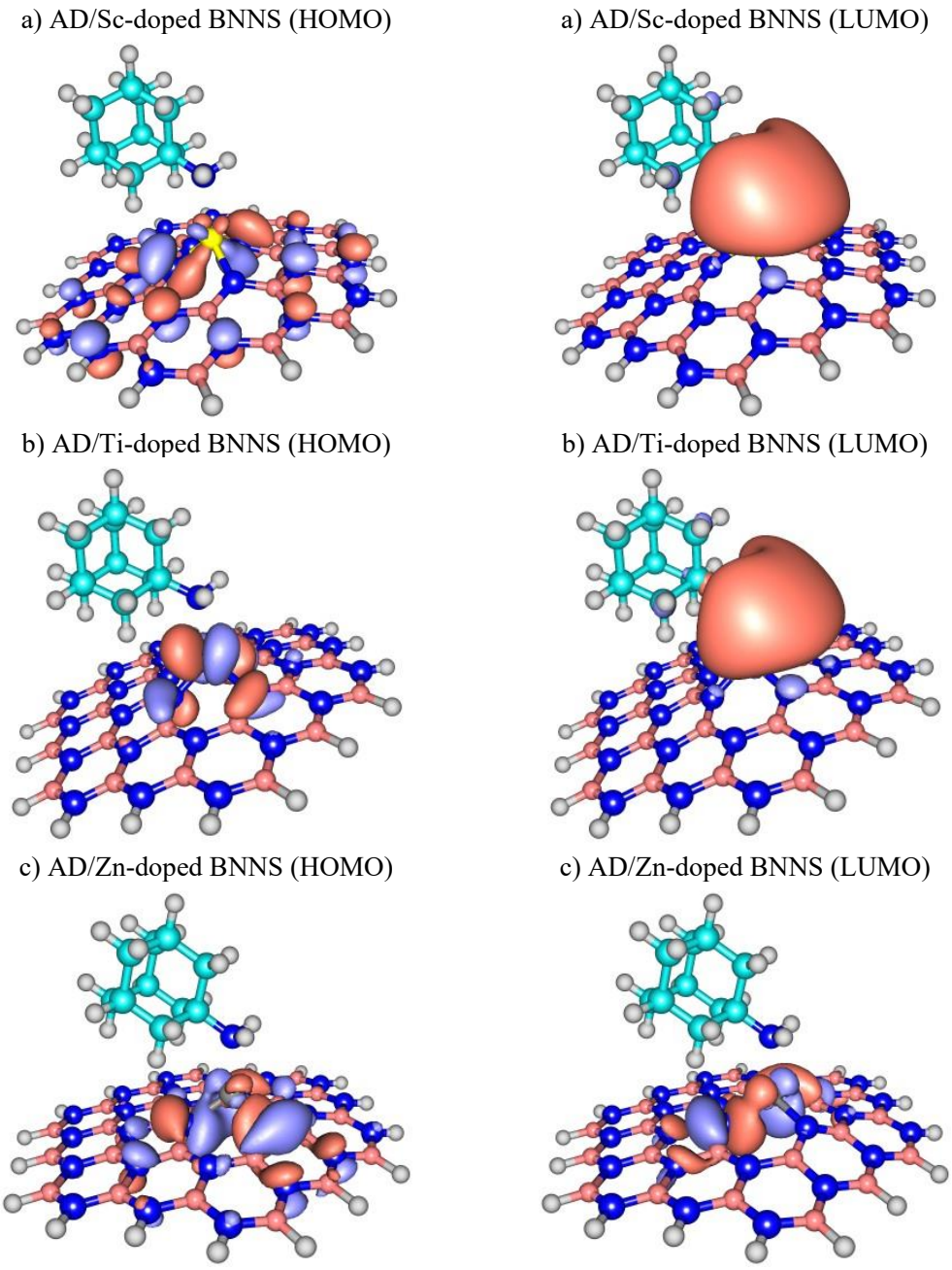

Fig. 8. The shape of HOMO and LUMO of the adsorption of amantadine on (a) Sc-, (b) Ti-, and (c) Zn-doped BNNSs

adsorption of amantadine on the doped BNNSs. Further, LP -> LP* 2e-stabilisation energies are in agreement with the adsorption energies. The results of the QTAIM analysis are summarized in Table 5. The density of all electrons (ρ), Lagrangian kinetic energy (G(r)), potential energy density (V(r)), and localized orbital locator (LOL) are employed for QTAIM analysis. The absolute ratio of V(r)/G(r) is more than 1, indictating the partial covalent nature of the nitrogen…zinc bond. However, the adsorption of amantadine on Zn-doped BNNS is weaker than its adsorption on Sc-, and Ti-doped BNNSs. The cause may originate from stronger LP to LP* delocalization and electrostatic interaction in N(AD)…Sc and N(AD)…Ti. The partial charges of the N atom of amantadine and transition metal are (+1.666, -0.947), (+1.493, -0.938), and (+1.306, -0.940) in CAM-B3LYP level for amantadine adsorption on Sc-, Ti-, Zn-doped BNNSs, respectively.

Fig. 7 displays the PDOS diagrams of amantadine/Sc-, Ti-, and Zn-doped BNNS complexes. Table 6 reportes the HOMO, LUMO, bandgap, and work function of the complexes. Comparing Table 6 to Table 1 demosntrates that the adsorption of amantadine on the doped BNNSs increases both HOMO and LUMO levels. The amantadine adsorption on Sc-doped BNNS significantly widened the bandgap energy of the nanosheet by raising the level of LUMO more than that of HOMO. The orbital decomposition analysis indicated that occupied p orbitals of N atom in the vicinity of Sc mainly dominate the HOMO of amantadine/Sc-doped BNNS, whereas the LUMO consists of unoccupied orbitals of Sc accompanied with unoccupied s orbitals of the amine group of amantadine (Fig. 8). The adsorption of amantadine on Ti- and Zn-BNNSs slightly widened the bandgap of the nanosheets. The electronic conductivity (σ) of materials is exponentially proportionate to their bandgap [27]:

$$\sigma \propto \exp\left(\frac{-E_g}{2kT}\right) \quad (11)$$

where K and T are Boltzmann constant and temperature, respectively. Based on Eq. (11), amantadine adsorption on Sc-doped BNNS distinguishably reduced the electron conductivity of Sc-doped BNNS. Therefore, Sc-doped BNNS can be utilized as an electronic conductivity sensor for amantadine. Additionally, the bandgap energy and the values of the work function of materials relate to some of their measurable properties. For example, the emitted current density (J_e) in thermionic emission is sensitive to the work function [28]:

$$J_e = -AT^2 \exp\left(\frac{-\Phi}{kT}\right) \quad (12)$$

where A indicates the Richardson constant. As shown in Table 6, the amantadine adsorption changes the work function of all of the considered doped BNNSs. Accordingly, Sc-, Ti-, and Zn-doped BNNSs are suitable work function type sensors for detecting amantadine.

The recovery time (τ) of adsorbents relative to attempt frequency (v_0) and temperature, can be obtained by the following equation [29]:

$$\tau = {v_0}^{-1} \exp\left({E_{bind}}/{KT}\right) \quad (13)$$

Based on this equation, for recycling Sc-, Ti-, and Zn-doped BNNS under visible and ultra-violent irradiation, a temperature of 500K is needed. Although these nanosheets aren't immediately reusable, they still can be employed as recyclable adsorbents and sensors of amantadine drug.

CONCLUSION

In the present work, the adsorption of amantadine drug on the Sc-, Ti-, and Zn-BN nanosheets was studied using B3LYP and CAM-P3LYP DFT functionals, NBO, and QTAIM. The energy and NBO calculations indicated that replacing a central B atom with Sc, Ti, and Zn atoms reduces the stability and bandgap energy of the nanosheet. Amantadine is chemically adsorbed on the transition metal dopant by its nitrogen atom. Among the considered doped BNNSs, Sc-doped BNNS was the best adsorbent for amantadine. Based on the QTAIM analysis, the interactions between amantadine and the doped BNNSs are strong non-covalent for (AD)N…Sc and (AD) N…Ti, and partial covalent for (AD)N…Zn. NBO analysis demonstrated that amantadine adsorption significantly widened the bandgap energy of Sc-doped BNNS; thus, Sc-doped BNNS can be used as an electronic conductivity type sensor of amantadine. Moreover, amantadine adsorption clearly changed the work function of the considered doped nanosheets. The calculated recovery times relative to frequency and temperature showed that used Sc-, Ti-, and Zn-doped BNNSs are recyclable under visible irradiation in 500K.

CONFLICT OF INTEREST

The authors declare no conflicts of interest.

REFERENCES

1. Boxall ABA. The environmental side effects of medication. EMBO reports. 2004;5(12):1110-6. https://doi.org/10.1038/sj.embor.7400307
2. Owens B. Pharmaceuticals in the environment: a growing problem. The pharmaceutical journal. 2015;294:7850.
3. Cussans A, Harvey G, Kemple T, Tomson M. Interventions to Reduce the Environmental Impact of Medicines: A UK perspective . The Journal of Climate Change and Health. 2021;4:100079. https://doi.org/10.1016/j.joclim.2021.100079
4. Kirschbaum J. Amantadine. In: Florey K, editor. Analytical Profiles of Drug Substances. 12: Academic Press; 1983. p. 1-36. https://doi.org/10.1016/S0099-5428(08)60162-8
5. Mosley C, Edwards T, Romano L, Truchetti G, Dunbar L, Schiller T, et al. Proposed Canadian Consensus Guidelines on Osteoarthritis Treatment Based on OA-COAST Stages 1-4. 2022;9. https://doi.org/10.3389/fvets.2022.830098
6. Siao KT, Pypendop BH, Stanley SD, Ilkiw JE. Pharmacokinetics of amantadine in cats. Journal of Veterinary Pharmacology and Therapeutics. 2011;34(6):599-604. https://doi.org/10.1111/j.1365-2885.2011.01278.x
7. Macchio GJ, Ito V, Sahgal V. Amantadine-induced coma. Archives of Physical Medicine and Rehabilitation. 1993;74(10):1119-20. https://doi.org/10.1016/0003-9993(93)90072-I
8. Gharibzadeh F, Vessally E, Edjlali L, Es haghi M, Mohammadi R. A DFT Study on Sumanene, Corannulene, and Nanosheet as the Anodes in Li–Ion Batteries. Iranian Journal of Chemistry and Chemical Engineering. 2020;39(6):51-62.
9. Afshar M, Ranjineh Khojasteh R, Ahmadi R, Nakhaei Moghaddam M. In Silico Adsorption of Lomustin anticancer drug on the surface of Boron Nitride nanotube. Chemical Review and Letters. 2021;4(3):178-84.
10. Mohammad Alipour F, Babazadeh M, Vessally E, Hosseinian A, Delir Kheirollahi Nezhad P. A Computational Study on the Some Small Graphene-Like Nanostructures as the Anodes in Na–Ion Batteries. Iranian Journal of Chemistry and Chemical Engineering. 2021;40(3):691-703.
11. Hashemzadeh B, Edjlali L, Delir Kheirollahi Nezhad P, Vessally E. A DFT studies on a potential anode compound for Li-ion batteries: Hexa-cata-hexabenzocoronene nanographen. Chemical Review and Letters. 2021;4(4):232-8.
12. Vessally E, Farajzadeh P, Najafi E. Possible Sensing Ability of Boron Nitride Nanosheet and Its Al- and Si-Doped Derivatives for Methimazole Drug by Computational Study. Iranian Journal of Chemistry and Chemical Engineering. 2021;40(4):1001-11.
13. Noroozi Z, Rahimi R, Solimannejad M. A computational study for the B30 bowl-like nanostructure as a possible candidate for drug delivery system for amantadine. Computational and Theoretical Chemistry. 2018;1129:9-15. https://doi.org/10.1016/j.comptc.2018.02.016
14. Farmanzadeh D, Keyhanian M. Computational assessment on the interaction of amantadine drug with B12N12 and Zn12O12 nanocages and improvement in adsorption behaviors by impurity Al doping. Theoretical Chemistry Accounts. 2018;138(1):11. https://doi.org/10.1007/s00214-018-2400-3
15. Sun X, Wan X, Li G, Yu J, Vahabi V. Amantadine antiparkinsonian drug adsorption on the AlN and BN nanoclusters: A computational study. Physics Letters A. 2020;384(5):126128. https://doi.org/10.1016/j.physleta.2019.126128
16. Doust Mohammadi M, Abdullah HY. Theoretical study of the adsorption of amantadine on pristine, Al-, Ga-, P-, and As-doped boron nitride nanosheets: a PBC-DFT, NBO, and QTAIM study. Theoretical Chemistry Accounts. 2020;139(10):158. https://doi.org/10.1007/s00214-020-02672-2
17. Mohammadi MD, Salih IH, Abdullah HY. An Ultimate Investigation on the Adsorption of Amantadine on Pristine and Decorated Fullerenes C59X (X=Si, Ge, B, Al, Ga, N, P, and As): A DFT, NBO, and QTAIM Study. Journal of Computational Biophysics and Chemistry. 2020;20(01):23-39. https://doi.org/10.1142/S2737416521500022
18. Becke AD. A new mixing of Hartree-Fock and local density functional theories. The Journal of Chemical Physics. 1993;98(2):1372-7. https://doi.org/10.1063/1.464304
19. Boys SF, Bernardi F. The calculation of small molecular interactions by the differences of separate total energies. Some procedures with reduced errors. Molecular Physics. 1970;19(4):553-66. https://doi.org/10.1080/00268977000101561
20. Yanai T, Tew DP, Handy NC. A new hybrid exchange-correlation functional using the Coulomb-attenuating method (CAM-B3LYP). Chemical Physics Letters. 2004;393(1):51-7. https://doi.org/10.1016/j.cplett.2004.06.011
21. Frisch M, Trucks G, Schlegel HJI, Wallingford. Gaussian 09w, Revison D. Gaussian. 2013.
22. Andrienko GJShwcc. Chemcraft-graphical software for visualization of quantum chemistry computations. 2010.
23. O'Boyle NM, Tenderholt AL, Langner KM. cclib: A library for package-independent computational chemistry algorithms. Journal of Computational Chemistry. 2008;29(5):839-45. https://doi.org/10.1002/jcc.20823
24. Bader RFW. Atoms in molecules. Accounts of Chemical Research. 1985;18(1):9-15. https://doi.org/10.1021/ar00109a003
25. Lu T, Chen F. Multiwfn: A multifunctional wavefunction analyzer. Journal of Computational Chemistry. 2012;33(5):580-92. https://doi.org/10.1002/jcc.22885
26. Zhu W, Esteban R, Borisov AG, Baumberg JJ, Nordlander P, Lezec HJ, et al. Quantum mechanical effects in plasmonic structures with subnanometre gaps. Nature Communications. 2016;7(1):11495. https://doi.org/10.1038/ncomms11495
27. Benramache S, Belahssen O, Guettaf A, Arif A. Correlation between electrical conductivity-optical band gap energy and precursor molarities ultrasonic spray deposition of ZnO thin films. Journal of Semiconductors. 2013;34(11):113001. https://doi.org/10.1088/1674-4926/34/11/113001
28. Grilj M, editor Thermionic emission. Seminar Report, University of Ljubljana; 2008.
29. Solimannejad M, Noormohammadbeigi M. Boron nitride nanotube (BNNT) as a sensor of hydroperoxyl radical (HO2): A DFT study. Journal of the Iranian Chemical Society. 2017;14(2):471-6. https://doi.org/10.1007/s13738-016-0994-8